# Effect of Polymeric Media on the Kinetics of Nanocluster Nucleation and Growth

**Nily Dan,*,† Melissa Zubris,‡ and Rina Tannenbaum‡,§**

*Department of Chemical and Biological Engineering, Drexel University, Philadelphia, Pennsylvania 19104; School of Materials Science and Engineering, Georgia Institute of Technology, Atlanta, Georgia 30332; and Department of Chemical Engineering, Technion, Israel Institute of Technology, Haifa, Israel*

*Received March 16, 2005; Revised Manuscript Received August 1, 2005*

ABSTRACT: The effect of a polymeric medium on the nucleation and growth kinetics of iron oxide ($\gamma$-$Fe_2O_3$) clusters is studied. We show that the kinetics in both poly(methyl methacrylate) and polystyrene are dominated by the nucleation stage, while the growth stage is largely suppressed. The rate constant is found to decrease with temperature. Most surprisingly, particles formed in a strongly adsorbing polymer, poly(methyl methacrylate), are shown to grow more slowly than those in a weakly interacting polymer, polystyrene. The kinetic mechanism is used to explain why the size distribution of nanoclusters formed in polymeric media is narrow when compared to particles synthesized in small molecule solvents.

## 1. Introduction

In many systems, sample size does not affect the material characteristics. However, in nanostructured materials, chemical activity and mechanical or optical properties are set by the (nano)domain size.[1] Controlling material properties requires, therefore, control of the nanodomain size and size distribution, since polydispersity in domain size implies polydispersity in material properties.

Recent studies have shown that conducting the synthesis of inorganic nanoclusters in polymeric media (either bulk/melt or solution) yields relatively narrow size and morphology distributions.[2−10] The synthesis procedure usually involves mixing an inorganic precursor (e.g., metal−carbonyl) into a polymeric suspension. Cluster formation is then triggered, commonly, by raising the temperature to initiate precursor decomposition and cluster formation.

Although the cluster size varies as a function of such parameters as the type of polymer, the polymer concentration (when conducted in solution), or system temperature,[2−10] the narrow size distribution seems to be a universal characteristic. For example, Gubin[3] showed that the size of Co particles formed in polyethylene is $3.6 \pm 1$ nm, while iron clusters formed in that matrix were on average $3.2 \pm 0.3$ nm. Similarly, we have shown[5] that $\gamma$-$Fe_2O_3$ clusters synthesized in melt polystyrene (PS) are $65 \pm 4$ nm, $25 \pm 3$ nm in polysulfone, and $10 \pm 2$ nm in poly(methyl methacrylate) (PMMA). It should be noted that, while the size of metal clusters formed in polymer solutions is known to depend on the polymer MW and concentration,[6] the size of particles formed in bulk polymeric media was found to be insensitive to the polymer MW for both PS and PMMA in the range $10^4$−$10^6$ g/mol.[5] The only exceptions to this rule of narrow size distributions in nanoparticles synthesized in polymeric media are systems where the inorganic content is high, but there the polydispersity has been traced to effects of flocculation.[5]

Although data to date suggest that the narrow size distribution in polymer-controlled cluster synthesis is relatively universal,[2−10] the mechanism by which the polymer "selects" a preferred nanocluster size has not been determined. One possibility is that the polymers "cap" or adsorb onto the particles once they reach a certain size, thereby prohibiting further growth.[3−6] Indeed, a mean-field model of equilibrium adsorption onto nanoparticles suggests that polymer adsorption is optimized on a specific nanoparticle radius.[5,6] The capping mechanism explains why the preferred radius of particles synthesized in bulk polymer is independent of the polymer MW, while particles formed in a polymer/solvent suspension vary nonmonotonically with the polymer length. It is also consistent with the observation that particle size is independent of the precursor initial concentration (below the flocculation threshold) and that cluster dimensions decrease with increasing polymer/particle compatibility.[3,5,6]

The capping mechanism, however, has one major flaw. Consider a system of inorganic precursor in a polymeric suspension. As the temperature is raised, the precursor decomposes and aggregation is initialized. Some stable clusters form at early times and grow until reaching the preferred size set by polymer adsorption and capping. New clusters continue to form—and grow—until they too reach the preferred size. Concurrently (in finite systems) the suspension is depleted of precursor. Eventually, the suspension is completely depleted of precursor, and nucleation and growth is stopped. This scenario suggests that, at any point in time, smaller clusters that did not have a chance to grow to the preferred (capping set) size will be observed. Yet, as discussed above, the size distributions are narrow in widely different systems, and particles that are much smaller than the average size are not observed.[2−10] Indeed, polydispersity in the particle size is as likely to be due to particles larger than the average size as to those smaller than that.[2−10]

To date, studies of nanocluster synthesis in polymeric suspensions tend to focus on the particle properties and

† Drexel University.
‡ Georgia Institute of Technology.
§ Technion, Israel Institute of Technology.
* Corresponding author: Ph (215) 895 6624, Fax (215) 895 5837, e-mail dan@cbis.ece.drexel.edu.

10.1021/ma050564t CCC: $30.25 
Published on Web 09/28/2005

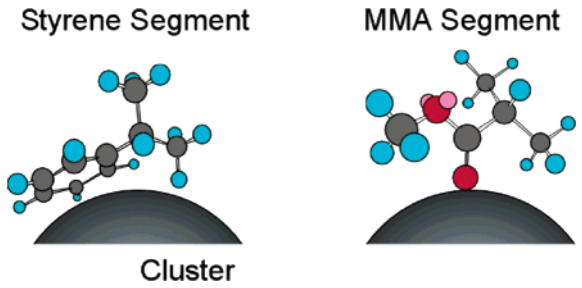


**Figure 1.** Cluster/polymer interactions: polystyrene (PS) adsorbs on metal surfaces through weak dipole−dipole interactions. Poly(methyl methacrylate) (PMMA) interacts with the metal surface through the coordination of the carbonyl groups on the acrylate side group, resulting in a relatively strong bond.

distribution at the end of the synthesis process. The goal of this paper is to study the kinetics of nanocluster nucleation and growth in polymeric suspensions, in an effort to identify the nucleation and growth stages and better understand the process by which the nanoclusters are formed. This understanding may suggest the underlying mechanism by which nanocluster formation in polymeric suspensions yields uniform clusters.

We follow the synthesis of iron oxide ($\gamma$-$Fe_2O_3$) nanoparticles from the decomposition of iron pentacarbonyl ($Fe(CO)_5$) in two different types of polymeric media: polystyrene (PS) and poly(methyl methacrylate) (PMMA). PS is known to adsorb onto metal surfaces through weak dipole−dipole interactions, while PMMA interacts with the metal surface through the coordination of the carbonyl groups on the acrylate side group, resulting in a relatively strong bond, as shown in Figure 1.

The decomposition reaction of $Fe(CO)_5$ leading to the formation iron clusters is initiated by the loss of at least one CO ligand in the iron precursor, followed by a cascade of ligand dissociation and complex rearrangements, giving rise to coordinatively unsaturated, multinuclear iron complexes, having a higher metal/ligand ratio than the original precursor.[6−9] These Fe "active" fragments, or "metallomers" (similar to the "mer"-based nomenclature for polymers), are highly reactive,[10,11] generating a nucleation and growth process that culminates in the formation of nanocrystals. In systems such as the case here, the presence of ambient oxygen leads to oxidation of the Fe "active" species to give rise to $Fe_2O_3$ particles:

$$Fe(CO)_5 \underset{K_{-1}}{\overset{T,K_1}{\rightleftharpoons}} Fe(CO)_{m\le 4} \underset{K_{-2}}{\overset{K_2}{\rightleftharpoons}} Fe_s \xrightarrow{O_2,K_3} \frac{1}{2}(Fe_2O_3)_s$$

where we neglect the released CO gas because it is flushed out of the system.

We find that, in both PS and PMMA, the decomposition rate of iron pentacarbonyl may be described as an exponentially decaying function with a characteristic decay time that decreases with increasing system temperature. The characteristic decomposition time is found to be significantly higher in the strongly interacting PMMA when compared to the weakly interacting PS.

To understand the kinetics of nanocluster formation in polymeric media, we compare the (theoretically calculated) rates of nucleation and growth. The exponential decay rate observed suggests that the system is dominated by the nucleation process and that growth is suppressed. As will be shown below, the ratio of nucleation to growth time scales is most sensitive to the value of the surface tension between the clusters and the media, which is a function of the chain MW;[12,13] in high-MW polymers, this ratio is much smaller than in oligomeric solvents, thereby suggesting that nucleation in these systems is rapid when compared to growth.

## 2. Materials and Methods

Sample preparation follows procedures previously published.[5,6] The polymer is mixed into an appropriate solvent, e.g. methylene chloride (Fisher Reagent), for 24−48 h at room temperature, followed by solvent drying using molecular sieve pellets (Matheson, Coleman and Bell). 1 mL of filtered iron pentacarbonyl (Alfa Products, Thiokol/Ventron Division) was added dropwise to the dried polymer film, mixed for ~5 min, and then film cast onto sheets of glass. All films were analyzed for iron content to determine actual $Fe(CO)_5$ retained. Systems examined included 5.0 g of polystyrene pellets (Polyscience, Inc., $\bar{M}_w$ = 159 400 g/mol) initially dissolved in 30.0 mL of toluene (Fisher-Reagent) at 50 °C and 5.0 g of PMMA pellets (Polyscience, Inc., $\bar{M}_w$ = 323 000) initially dissolved in 32.2 mL of chlorobenzene (Fisher-Reagent).

Thermal decompositions were carried out in a temperature-controlled vacuum oven with controlled atmosphere capability. Decomposition times and temperatures were varied for kinetic measurements. The rate of iron oxide cluster formation was measured by infrared spectroscopy on a Nicolet MX-1 and a Nicolet Nexus 870 Fourier transform infrared spectrophotometers. We monitored the increase in the intensity of the asymmetric Fe−O stretching vibration of $\gamma$-$Fe_2O_3$ at 520 $cm^{-1}$,[14−16] yielding the infrared profile shown in Figure 2a. The rate of precursor decomposition was determined by monitoring the variations in the intensity of the two strong absorption bands at 2019 and 1996 $cm^{-1}$, corresponding to the asymmetric and symmetric stretching vibrations of the carbonyl groups in a hydrocarbon solvent (Figure 2b) and in the various polymeric matrices used in the study (Figure 2c). The slight shift to lower wavenumbers of the carbonyl absorption bands in the polymeric medium is attributed to the restriction in the mobility of the iron carbonyl species in the polymer matrix. The carbonyl stretching band at 1996 $cm^{-1}$, which was observed to change during decomposition of the $Fe(CO)_5$−polymer films, was used to follow the kinetics and subsequently was also used for the calculation of the activation energies for the thermal decomposition reactions in the composite films. The absorptions of the infrared carbonyl stretching band at 1996 $cm^{-1}$ for polymer films with different iron carbonyl initial standardized concentrations were used to calculate the extinction coefficient, $\epsilon$, for $Fe(CO)_5$ in the various polymers through the relationship $A_{abs} = d\epsilon_i\phi_i$, where $d$ is the optical path, $\epsilon_i$ is the molar absorptivity of a given species at a specific wavenumber, and $\phi_i$ is the molar concentration of a given species in the system.[20]

Decompositions of $Fe(CO)_5$ in a hydrocarbon solvent, e.g., ethylbenzene, in the absence of polymer were measured at different temperatures and followed by infrared spectroscopy in sealed demountable liquid cells equipped with either NaCl or KBr polished crystals. Ethylbenzene (Fisher, spectroscopic grade) was used as a reference. The molar extinction coefficient was calculated by constructing a calibration curve, and the value of 8000 L $mol^{-1}$ $cm^{-1}$ was used for determination of $Fe(CO)_5$ initial concentration in the ethylbenzene solution.

## 3. Results

The process of iron oxide nanocluster formation may be divided into two steps: the formation of active Fe fragments due to the loss of CO ligand(s) and aggregation of such active fragments into the stable iron oxide nanoparticles.

Optimally, to measure the rate of nanocluster formation, we would follow cluster growth through the IR peak associated with the iron oxide at 520 $cm^{-1}$. Unfortunately, this characteristic absorption band resides

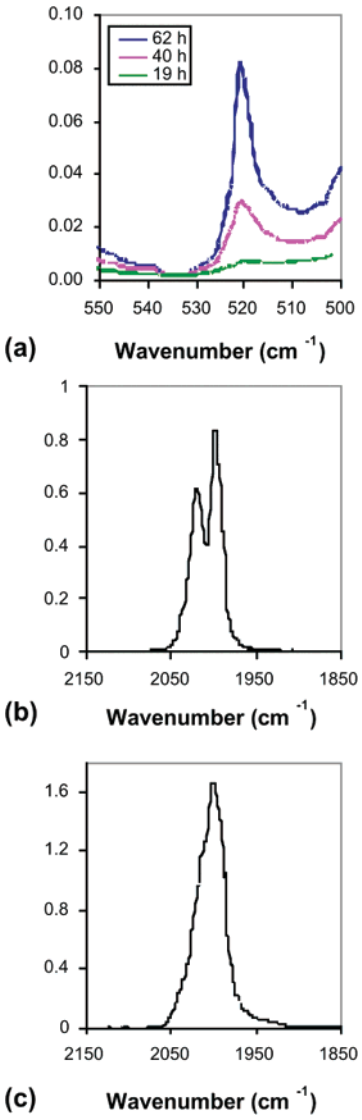


**Figure 2.** Infrared absorption spectra of iron carbonyl (precursor) and iron oxide (cluster) in the reaction medium: (a) The increase in the FTIR signature absorption bands of $\gamma$-$Fe_2O_3$, specifically the asymmetric Fe−O stretch at 520 $cm^{-1}$, as a function of reaction progress. (b) Infrared spectrum of $Fe(CO)_5$ precursor in pure hydrocarbon solvent (toluene, $CH_3C_6H_5$) prior to decomposition. (c) Infrared spectrum of $Fe(CO)_5$ precursor in a polystyrene film, prior to decomposition.

at the lower end of the mid-IR range of our instruments and hence is susceptible to artifacts due to beam cutoff.[17,18] On the other hand, the rate of precursor decomposition can be clearly monitored through the decrease in the intensity of the carbonyl absorption bands of $Fe(CO)_5$ (see Figure 2). However, to use the rate of precursor decomposition as a measure of nanocluster synthesis, we must be able to relate the two. As described in eq 1, iron cluster formation involves several steps. Since iron atoms are confined to the system (and cannot, for example, evaporate as a gas), we can use a simple mass balance on the iron atoms to relate the different species' molar concentrations. The precursor concentration (which we will denote by $\phi_5$), the unstable species (defined as $\phi$), and the solid nanoclusters ($\phi_s$)

$$m_{Fe}(\phi_5 + \phi + \phi_s) = m_{Fe}\phi_0 \qquad (2)$$

where $\phi_0$ is the initial (molar) concentration of precursor in the system, a known parameter, and $\phi_5(t)$ is measured as described in Figure 2. $m_{Fe}$ is the MW of Fe atoms. Thus, to evaluate the rate of solid nanocluster formation ($\partial\phi_s/\partial t$), we need to be able to measure the concentration of the unstable species, $Fe(CO)_m$, where $m < 5$, or $Fe_x(CO)_y$, where $x/y \leq 4$.

When the decomposition of $Fe(CO)_5$ is conducted in oligomeric media (i.e., solvents), it is possible to observe the formation and temporary accumulation of $Fe_3(CO)_{12}$ ($x/y = 4$), as suggested by the appearance of its characteristic carbonyl stretch at 2046 $cm^{-1}$ (see Figure 3a).[19,20] Under the specific experimental conditions $Fe_3(CO)_{12}$ behaves as a metastable multinuclear carbonyl complex and further loses a carbonyl ligand to generate unsaturated, unstable, and reactive species that drive the formation of the iron "metallomers". However, Figure 3b shows that when the decomposition of $Fe(CO)_5$ is conducted in either of the bulk polymeric media used in this work (PS and PMMA), the appearance of this intermediate is not observed, regardless of the decomposition temperature. We conclude that the lack of an FTIR peak at 2046 $cm^{-1}$ when the synthesis is conducted in a polymeric environment is due to the fact that the concentration of $Fe_3(CO)_{12}$ (and thus any other intermediary species) remains below the detection limit of the FTIR ($\leq 10^{-6}$ M). This implies that $\phi \approx 0$, which leads (via the rearrangement of eq 2) to $\phi_s \approx \phi_0 - \phi_5$.

One may speculate that even if the concentration of $Fe_3(CO)_{12}$, $\phi$, is low, $\partial\phi/\partial t$ may be large. In that case, $\partial\phi_s/\partial t \neq -\partial\phi_5/\partial t$, and we could not determine the rate of cluster formation from the precursor decomposition rate. However, $\partial\phi/\partial t$ defines the net accumulation of the intermediate species, namely, the difference between its rate of formation through $Fe(CO)_5$ decomposition and rate of decomposition to the stable iron cluster. If the net rate is positive, we should see some accumulation of the intermediate species over time; yet, even at long times after the initiation of the process, we do not see the characteristic peak at 2046 $cm^{-1}$. A negative value of $\partial\phi/\partial t$ indicates that the rate of cluster formation is higher than the rate of precursor decomposition, in which case cluster formation would be suppressed rapidly by the depletion in the intermediate species.

The absence of detectable amounts of intermediate species throughout the experiment suggests that the rate of nanocluster formation, $\partial\phi_s/\partial t$, is equal (and opposite in sign) to the decomposition rate of the precursor, $\partial\phi_5/\partial t$. To examine this conclusion, we compare the relative absorbance of the $Fe(CO)_5$ peak, as a function of time, to that of the $Fe_2O_3$ in one particular system (Figure 3c): Both absorbance values are normalized by their highest value (which in the case of the precursor means the initial value, while for the cluster it is the final value at long times). As discussed above, the intensity of the species' characteristic infrared absorption band $A_{abs}$ is linearly proportional to the molar concentration of the species,[20] so that the rate of change of the normalized absorbance, $\partial(A(t)/A_0)/\partial t$ is equal to $\partial\phi/\partial t$.

Comparing the rate coefficients for precursor decomposition ($\partial\phi_5/\partial t$) to that of solid formation($\partial\phi_s/\partial t$), we see that the two are opposite it sign and equal in magnitude, thereby strengthening our claim that the rate coefficients for both the decomposition of $Fe(CO)_5$, $K_1$, and formation of $Fe_2O_3$, $K_3$, are comparable.

Since we established that $\partial\phi_s/\partial t \approx -\partial\phi_5/\partial t$, we can now perform the quantitative kinetic analysis based on the effective molar extinction coefficients of $Fe(CO)_5$ at the

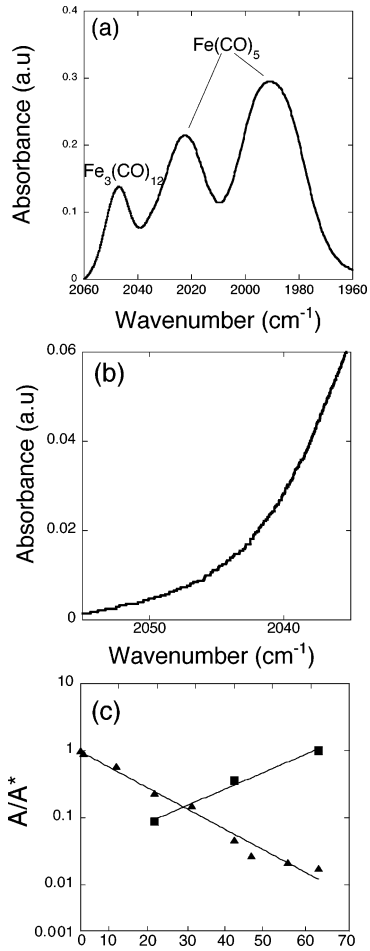


**Figure 3.** Determination of the relationship between the decomposition of $Fe(CO)_5$ and formation of $Fe_2O_3$: (a) The absorbance spectrum of a decomposing solution of $Fe(CO)_5$ in ethylbenzene at 132 °C, showing the characteristic $Fe(CO)_5$ absorption bands at 1996 and 2021 $cm^{-1}$ and a new band at 2046 $cm^{-1}$, identified as belonging to $Fe_3(CO)_{12}$, corresponding to the asymmetric stretch of the terminal carbonyl groups. (b) IR spectra of $Fe(CO)_5$ decomposition in PMMA (at 132 °C) in the 2046 $cm^{-1}$ range; we see the absence of any peak characteristic of $Fe_3(CO)_{12}$. The peak is not detectable in either PS or PMMA at all the temperatures and time scales examined in this study. Note that, in comparison, this peak is extremely visible for iron pentacarbonyl decomposition in ethylbenzene (a). (c) Comparison of the absorbance of $Fe(CO)_5$, normalized by the absorbance value ($A^*$) at $t = 0$ (triangles) and $Fe_2O_3$, normalized by the value ($A^*$) of absorbance at $t \approx 65$ h (squares), as calculated on the basis of the relative intensity of their characteristic infrared absorption bands in PMMA (at 132 °C). As discussed in the text, $A/A^*$ is an indicator of the relative concentration of each species. Error bars are smaller than the symbol size. The lines describe a fit to an exponential function (see the discussion for Figure 4). We find that the normalized absorbance, a measure of concentration, of the precursor $Fe(CO)_5$ scales as $e^{-0.07t}$, while that of the $Fe_2O_3$ scales as $e^{0.06t}$. Thus, the rates of precursor decomposition and cluster formation are approximately equal, $-\partial\phi_5/\partial t = 0.07 \approx \partial\phi_s/\partial t = 0.06$, as expected from the fact that there is no detectable amount of intermediates (unstable species).

1996 $cm^{-1}$ band. In Figure 4 we plot the decrease in the iron carbonyl volume fraction in the two polymeric matrices: poly(methyl methacrylate) (PMMA) and polystyrene (PS). We see that the precursor decomposes faster as the temperature increases, in both types of media, suggesting an endothermic process. Also, the precursor decomposes faster in PS than in PMMA, as indicated by the characteristic time scale required to reduce the precursor concentration by a fixed fraction.

## 4. Kinetic Model

The data presented in Figure 4 show the decay rate of the precursor, $\partial\phi_5/\partial t$, which we have shown corresponds to the rate of solid formation, $-\partial\phi_s/\partial t$. Although we can draw some qualitative conclusions (e.g., that increasing the temperature increases the decomposition and thus solid formation), quantitative analysis of the rate of precursor decay and thus of cluster formation requires understanding of the relationship between cluster formation and time and its effect on the rate of precursor degradation.

The kinetics of nucleation and growth have been extensively studies (see, for example, refs 19−23). However, most previous studies assume infinite reservoir, where $\phi_5$ remains constant with time, and thus do not directly apply to our closed system.[19−23] Thus, we adapt here the traditional nucleation and growth models to account for the finite precursor concetration (namely, its depletion with time), as well as the fact that the nanoclusters formed are extremely uniform in dimeter.[2−10]

Cluster formation is divided into two stages: First is the nucleation stage, where a critical number of atoms come together to form a stable (critical) nucleus. Clusters smaller than the critical size dissolve, while clusters larger than the critical size are stable. The second stage is the growth stage, where the stable nuclei grow through the addition of more atoms.[19−23] Classical models for homogeneous nucleation and growth suggest that the energy of an embryonic inorganic cluster of volume $V$ and surface area $A$ is dominated by a combination of the "bulk" energy (which is given by the interaction energy gain due to association of the atoms, or "monomers") and the interfacial tension with the surrounding media:

$$F = -\epsilon V + \gamma A \tag{3}$$

where $F$ is the free energy of a given embryonic cluster, $\epsilon$ is the net interaction energy associated with moving an inorganic molecule from the environment into the cluster (given on a per volume basis), a function of the chemical potential difference between the two states and, thus, of the inorganic molecule concentration, and $\gamma$ is the interfacial tension between the particle and its environment. For a spherical cluster, the critical nucleus size $r^*$ and the barrier for the critical nucleus formation $F^*$ are given by

$$r^* = \frac{2\gamma}{\epsilon} \tag{4a}$$

$$F^* = \frac{16\pi\gamma^3}{3\epsilon^2} \tag{4b}$$

Clusters whose size is smaller than $r^*$ will dissolve, since the energy gain due to association is smaller than the energy loss due to formation of an interface. Clusters larger than $r^*$ will continue to grow, since the interfacial penalty is smaller than the gain due to addition of more "monomers", or molecules.

The rate of stable nuclei formation (per unit volume) may be related to the energy barrier height, $F^*$, through the Boltzmann relationship

$$\frac{d\hat{n}}{dt} \approx \alpha\phi e^{-F^*/kT} \tag{5}$$

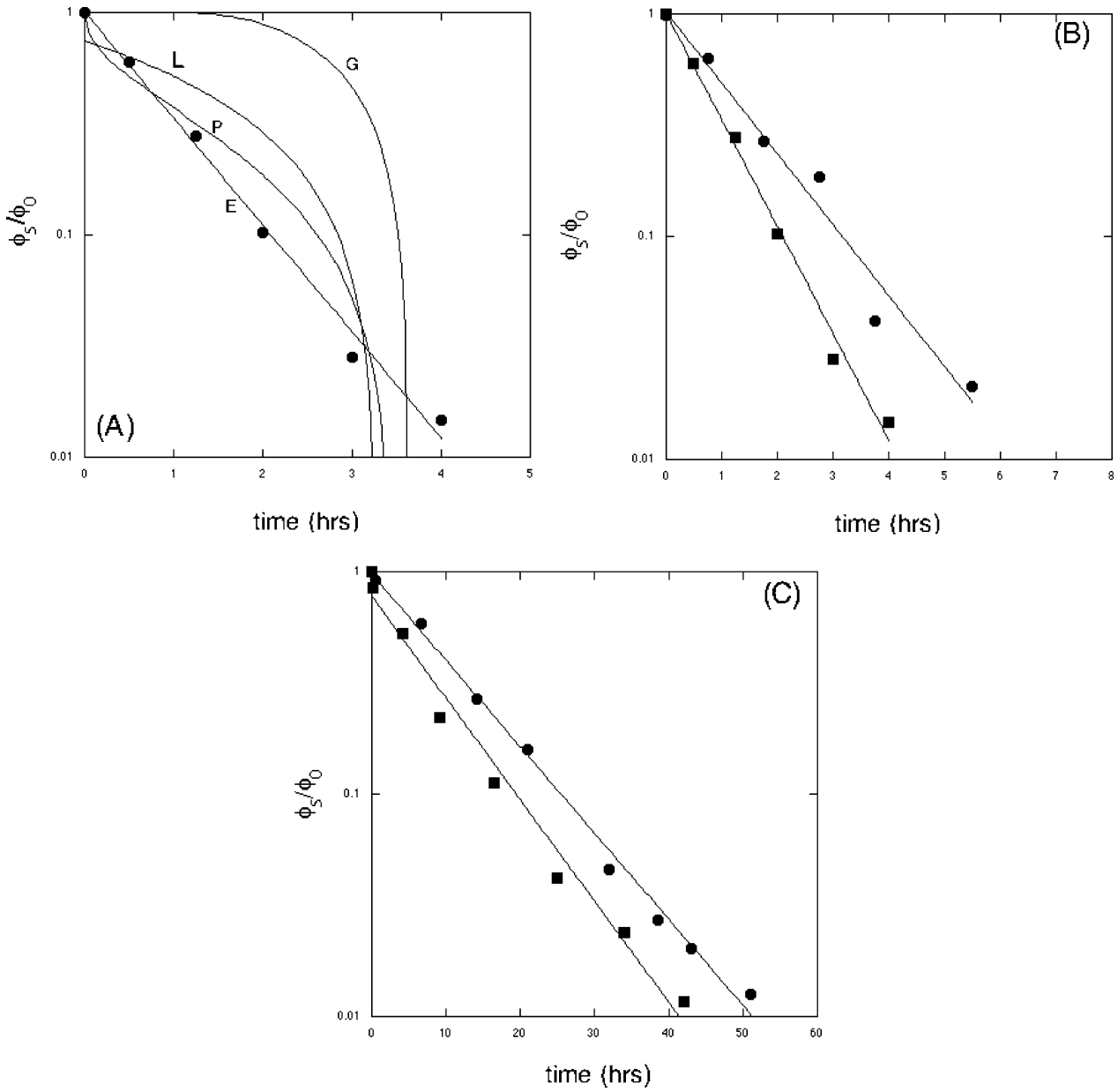


**Figure 4.** Normalized volume fraction of $Fe(CO)_5$, $\phi_5$, as a function of time. (a) $Fe(CO)_5$ in PS in 143 °C. Data fits shown include linear (L), power law (P), and growth dominated (G) as in eq 11 and exponential (E), as given by eq 9. We see that only the exponential fit captures the correct trends. (b) $Fe(CO)_5$ in PS for $T = 138$ °C (circles) and $T = 143$ °C (squares). Both temperatures are above the polymer $T_g$. Error bars are smaller than the symbol size. Lines describe a fit to an exponential decay, as predicted from the nucleation-dominated analysis (eq 9). (c) $Fe(CO)_5$ in PMMA for $T = 138$ °C (circles) and $T = 143$ °C (squares). Both temperatures are above $T_g$. Error bars are smaller than the symbol size. Lines describe a fit to an exponential decay function.

where α is a rate constant, a function of the diffusion coefficient of atoms in the media ($D$), $\tilde{n}$ is the number of clusters per unit volume, $k$ is the Boltzmann constant, and $T$ is the temperature. The linear dependence of the nucleation rate on $\phi$, the concentration of unstable species, reflects the fact that the probability of atoms coming together to form a critical cluster increases with the concentration of the (unstable) species.

Once a stable cluster, or nucleus, is formed, it may grow through two mechanisms: (a) molecular species addition and/or (b) aggregation with other nuclei. The rate of molecular addition is dominated by molecular transport through the suspension media (namely, diffusion). Aggregation is a more complex process, since it depends on both the rate of transport of the clusters and the strength of cluster−cluster interactions, and has been shown[2−10] to be negligible in systems where the metal volume fraction was low—as in the cases studied in this paper. Moreover, aggregation of clusters does not affect the (measured) concentration of iron oxide or the depletion in precursor concentration.

Cluster growth through molecular addition is controlled by the diffusional flux to the clusters. The full diffusion/growth problem is complex and cannot be solved analytically, since it involves a moving boundary—the cluster radius—as well as a time-dependent diffusant concentration. However, applying a simplified approach, we can define the flux to the growing cluster through a "boundary layer", where the concentration of unstable iron molecules at the cluster interface is zero, and outside the boundary layer it is given by the average suspension concentration. The increase of the cluster radius $r$ with time is roughly given then by

$$\frac{dr}{dt} \approx \frac{D}{L}\phi \tag{6}$$

where $D$ is the diffusion coefficient of the unstable species in the media and $L$ the characteristic length scale of the diffusion boundary layer thickness.

Combining the nucleation and the growth rates, we get for the overall concentration (or volume fraction) of the solid clusters

$$\phi_s = \int_0^t \int_{t'}^t \frac{d\hat{n}}{dt}\Big|_{t'} r^2 \frac{dr}{dt}\, dt'\, dt \tag{7}$$

where clusters nucleated at time $t'$ grow through the diffusion process over the period $(t - t')$.

When the concentration of iron pentacarbonyl is constant (e.g., an infinite reservoir), the rates of new nuclei formation and growth are constants as well. If $dr/dt$ is constant (see eq 6), $r(t)$ scales as $t$, and eq 7 yields a cluster formation rate that scales as $t^2$, which translates to a precursor decay rate that scales as $-t^2$. However, it is clearly seen (Figure 4) that the rate of cluster formation, or iron pentacarbonyl decay, cannot be described by such a function.

Moreover, if nucleation and growth have similar rates, then the resulting clusters must be polydisperse: As shown in Figure 5, clusters formed initially can grow to larger sizes than clusters formed at later stages. This is exacerbated by the continuous depletion of the precursor, which would further suppress the growth of clusters formed at long time when compared to those (already large ones) nucleated initially.

On the other hand, if one rate dominates (Figure 5), then the cluster distribution will be narrow: If nucleation is rapid but growth is slow in comparison, then (regardless of when a cluster was formed) all clusters will remain more or less at the critical cluster size, $r^*$. On the other hand, if nucleation is slow when compared to growth, the clusters formed initially will rapidly grow and deplete the suspension, thereby suppressing further nucleation. Obviously, this analysis is overly simplified and idealized, but it allows us to calculate rate constants applicable to these two limits.

In the case where the nucleation rate dominates (namely, growth is suppressed), $r$ remains constant at $r^*$, so that eq 7 may be written as

$$\phi_s \approx \phi_0 - \phi_5 = \int_0^t \frac{d\hat{n}}{dt}\Big|_t \frac{4\pi d r^{*3}}{3}\, dt \sim \int_0^t k_e a \phi_5 r^{*3} e^{-F^*/kT}\, dt \tag{8}$$

for simplicity we neglect numerical coefficients such as $(4\pi/3)$. This yields a classical exponential decay:

$$\frac{\phi_5}{\phi_0} \approx e^{-t/\tau} \tag{9a}$$

where $\tau$ is the characteristic nucleation time, equal to

$$\tau = \frac{1}{a k_e r^{*3} e^{-F^*/kT}} = \frac{1}{a k_e r^{*3}} e^{F^*/kT} \tag{9b}$$

Large values of $\tau$ indicate slow nucleation, and thus decomposition rate, while a low value of $\tau$ describes a rapid decrease in the iron−carbonyl concentration due to rapid nucleation.

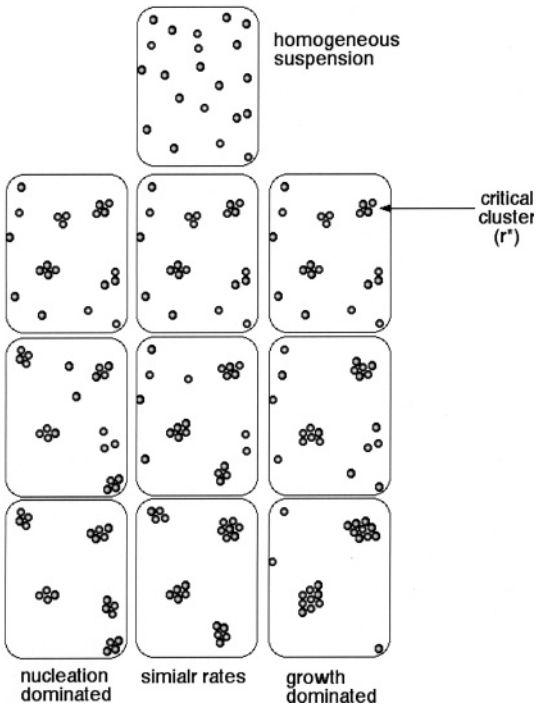


**Figure 5.** Effect of nucleation and growth rates on the nancluster size distribution. The dark spheres denote the dispersed molecular species. Stable nuclei ($r^*$) are taken, in this system, to be 4 molecules (or atoms) large. In the nucleation dominated regime (left), clusters that are smaller than 4 units dissolve, while those that are equal to 4 units remain stable. However, since the growth rate is much slower than the nucleation rate, the suspension is depleted before significant growth occurs, thereby leading to a uniform distribution of clusters of size 4. In systems where both rates are similar (center), nucleation and growth occur simultaneously. As a result, clusters formed initially grow to be much larger than those nucleated at later stages, and the cluster size distribution is large. When the growth rate dominates (right), nucleation takes place only initially. Once some nuclei formed growth takes place, rapidly depleting the suspension and inhibiting further nucleation. The resulting clusters are relatively uniform in size.

In the opposite regime, $F^*/kT$ is very large so that $\tilde{n}$ remains constant (at the initial value $\hat{n} \sim \phi_0 e^{-F^*/kT}$) and does not increase with time. The reduction in the iron−carbonyl concentration is therefore dominated by the diffusional flux to the clusters. (Note that cluster growth by flocculation will not affect the concentration of the iron−carbonyl atoms.) Assuming that all clusters are (more or less) similar in size, the depletion in the iron−carbonyl volume fraction is equal to the volume of the growing clusters:

$$\phi_s \approx \phi_0 - \phi_5 = \frac{4\pi}{3}\hat{n} r(t)^3 \tag{10}$$

This leads to (assuming that $r^*$ is small)

$$r(t) \sim \sqrt{e^{2t/\beta}} - 1 \tag{11a}$$

$$\frac{\phi_5}{\phi_0} \approx 1 - (\sqrt{e^{2t/\beta}} - 1)^3 \tag{11b}$$

where the characteristic decay time scale here is given by $\beta = L/D\phi_0^{2/3}(4\pi\hat{n}/3)^{1/3}$. Note that, unlike the decay rate associated with the nucleation process ($\tau$), which is independent of $\phi_0$, $\beta$ is inversely proportional to the

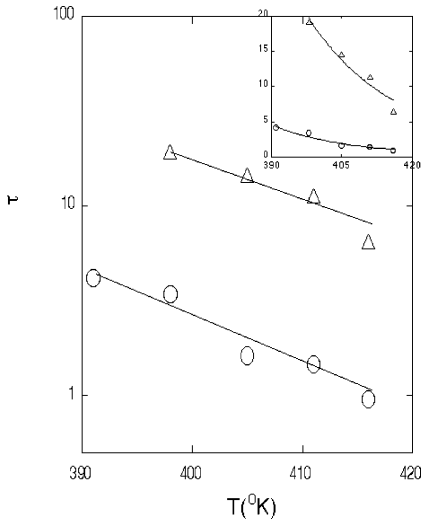


**Figure 6.** Nucleation time constant ($\tau$) as a function of system temperature in PMMA (triangles) and PS (spheres). All temperatures are above the $T_g$ of either polymers. The rate constants were calculated from a fit of the data to an exponentially decaying profile, as shown in Figure 4. We see that the decay rate in PMMA is always higher than in PS, indicating a slower decomposition rate. The lines describe a fit to the function $Ae^{B/T}$. For PMMA, $A \approx 2.5 \times 10^{-8}$ and $B \approx 8980$. For PS, $A \approx 4.6 \times 10^{-10}$ and $B \approx 8100$. According to eq 9b, $A$ scales as $1/r^{*3}$, suggesting that the ratio of the PS critical nucleus size to that of the PMMA is approximately $(2.5 \times 10^{-8}/4.6 \times 10^{-10})^{1/3} = 3.8$. Previous studies[5] have shown that the ratio between the equilibrium cluster sizes in PS and PMMA is 3.25.

initial iron−carbonyl volume fraction. Thus, growth occurs more rapidly in systems with higher precursor concentrations. The average volume of the clusters is therefore given by the overall amount of precursor ($V\phi_0$, where $V$ is the suspension volume) divided by the number of nuclei, $\hat{n}$. Since in this limit the nuclei form only initially before significant precursor depletion occurred, $\hat{n} \sim \phi_0$ (eq 5). As a result, the average size of the clusters is expected to be insensitive to precursor concentration.

## 5. Discussion

The synthesis of metal nanoclusters in polymeric media is known to yield narrow cluster size distributions.[2−10] In this paper we examine the kinetics of iron oxide nanocluster formation in polymeric (bulk) media by following the decomposition rate of the precursor, iron pentacarbonyl. The rate of precursor decomposition can be used to determine the rate of colid cluster formation, since we show that the concentration of intermediate species is negligible (Figure 3).

We suggest that a uniform, or monodisperse, cluster population can be obtained only if either nucleation or growth dominates cluster formation (see Figure 5). Similar rates for these two stages will yield a polydisperse distribution.

In Figure 4 we attempt to fit our data to the rate functions derived for the two stages. We see that the decomposition rate is successfully described by the exponential decay function for both polymers at all the temperatures examined and that large deviations are seen when attempting to use the growth function (or, indeed, extraction of the nucleation rate constants yields (see Figure 6) that the rate constants for both PS and PMMA decrease with temperature, namely, the rate of nucleation increases with increasing temperature.

If the rate of nucleation dominates, eq 9b suggests that the temperature dependence of the characteristic time constant, $\tau$, scales as $e^{F^*/kT}$. The values of the fitting parameters may be used to yield quantitative information regarding the system (assuming for simplicity that the transport rate in both polymers, $\alpha$, is similar): The prefactor to the exponential should correspond, according to eq 9b, to $1/(\alpha r^{*3})$, thereby suggesting that $(r^*_{PS}/r^*_{PMMA})$ should be equal to $\approx 3.8$. Previously, we measured the equilibrium size of iron oxide nanoclusters synthesized in the two types of polymers,[5] finding that the cluster size in PS is $65 \pm 4$ nm and $20 \pm 2$ nm in PMMA (independent of temperature or precursor concentration); namely, their ratio is $\sim 3.25$—quite similar to the one predicted by the nucleation-dominated model. The nucleation energy barrier, $F^*$, is found to be slightly lower for PMMA than for PS (a factor of $\sim 0.9$), also as may be expected from the fact that the interactions between PMMA and the iron clusters are more favorable than those of PS.

Equation 9b also helps explain why the characteristic time scale for the precursor depletion is higher (slower) in PMMA than in PS: the significant parameter setting the rate is the surface tension between the nucleating particles and the surrounding media. In PMMA, the interactions are more favorable than in PS, leading to smaller surface tension, smaller equilibrium particles, and slower decomposition rates.

Our results thus far are consistent with the supposition that in polymeric media the nucleation rate is much faster than growth rate. Note that this does not necessarily imply fast kinetics; indeed, we find that the characteristic time scales may be on the order of hours, but it does means that growth would be even slower. In small molecule solvents, the wide range of particle sizes suggests that the two rates are comparable (see Figure 5). Why then is nucleation faster, when compared to growth, in polymeric media but not in small molecule solvents?

To answer this, we need to compare the ratio of the characteristic time scales for nucleation and for growth,

$$\frac{1}{ar^{*3}e^{-F^*/kT}} \ll \frac{L}{D\phi_0 e^{-F^*/3kT}} \tag{12a}$$

$$\frac{e^{32\pi\gamma^3/9\epsilon^2 kT}}{(2\gamma/\epsilon)^3} \ll \frac{\alpha L}{D\phi_0} \tag{12b}$$

where we have used the relationship $\hat{n} \sim \phi_0 e^{F^*/kT}$ and neglected numerical coefficients of order 1.

One issue that may significantly differentiate the rates of nucleation and growth in oligomers when compared to polymeric media is the transport rate of small molecule (precursor, unstable) species. The transport rate of molecular species in polymeric melts is well-known to be much slower than in small molecule solvents.[23] However, both $\alpha$ and $D$ are rate constants describing the transport of molecular species in the media. Thus, it is reasonable to expect that, although their magnitudes are smaller in polymers than in solvents, their ratio will be largely unchanged. We also expect the thickness of the diffusion layer ($L$) and the energy of metal atom association ($\epsilon$) to be similar in small molecule and polymeric media of similar chemistries (e.g., PS and styrene or toluene).

Combining these, we reach the following conclusion: The ratio of the nucleation and growth time scales is

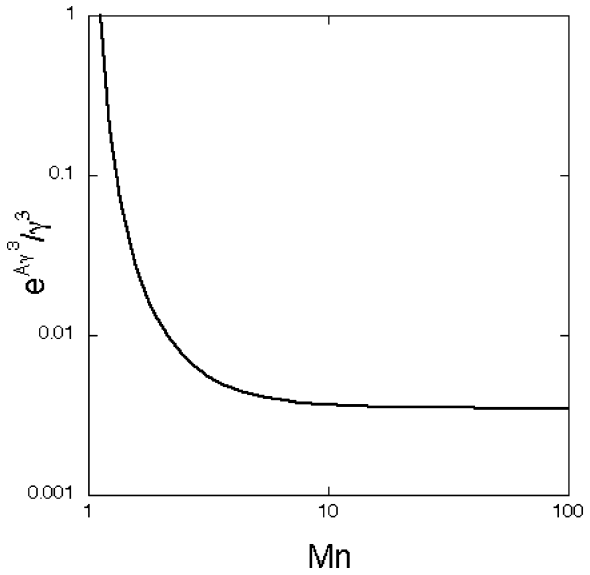


**Figure 7.** Effect of chain MW on the ratio of the nucleation time scale to growth time scale (eq 12). We use the correlation $\gamma = \gamma_0 - \gamma_1/M_n$, as suggested in the literature.[12,13] $A = 32\pi/9\epsilon^2$. All constants are taken to be equal to 1 for simplicity, and the $y$ axis is normalized by the value at MN = 1. We see that the ratio of the two time scales decreases significantly with increasing chain MW, thereby suggesting that in high MW systems the rate of nucleation becomes smaller when compared to growth.

set by the interfacial tension between the media and the nucleating clusters. For nucleation to be more rapid that growth $e^{32\pi\gamma^3/9\epsilon^2 kT}$ must be small relative to some constant ($8\alpha L/D\epsilon^2\phi_0$), while high values of this exponential factor indicate similar rates.

The surface tension of polymers varies as $\gamma = \gamma_0 - \gamma_1/M_n$ or as $\gamma_0 - \gamma_2/M_n^{2/3}$, where $M_n$ is the polymer molecular weight.[12,13] In Figure 7 we plot the ratio of the nucleation to growth time scales as a function of $M_n$: we see that the ratio of the rates is high in the limit of low molecular weights and decreases as the molecular weight increases. Thus, in high-MW media, the ratio between the characteristic time scale for nucleation to growth is expected to be smaller than in the equivalent oligomeric solvent, thereby leading to the dominance of the nucleation stage.

In conclusion, we examine here the kinetics of iron oxide nanocluster synthesis in polymeric media. We follow the rate of precursor decomposition as a function of time and decomposition temperature, as a measure of the cluster formation rate. We find that in both PS and PMMA, at all temperatures examine, the system is dominated by the nucleation stage and that growth is largely suppressed. The rapid rate of nucleation, when compared to growth, is linked to the effect of chain MW on the surface tension between the polymeric media and the nanoclusters.

**Acknowledgment.** This work was supported by the Petroleum Research Fund of the American Chemical Society, PRF #40014-AC5M, and by DARPA, Contract F33615-01-C-5023**.** The authors thank Drs. M. Levy and S. Reich (the Weizmann Institute of Science, Rehovot, Israel) and Dr. E. Goldberg (University of Florida, Gainesville, FL) for contributions to earlier studies and to Ms. Marcela Anghelovitz for her help with the initial calculations of reaction rate constants.

## References and Notes

(1) Tang, J. G.; Hu, K.; Liu, H. Y.; Guo, D.; Wu, R. J. *J. Appl. Polym. Sci.* **2000**, *76*, 1857.
(2) Kane, R. S.; Cohen, R. E.; Silbey, R. *Chem. Mater.* **1999**, *11*, 90.
(3) Gubin, S. P. *Colloids Surf., A* **2002**, *202*, 155.
(4) Kane, R. S.; Cohen, R. E.; Silbey, R. *Langmuir* **1999**, *15*, 39.
(5) Tannenbaum, R.; Zubris, M.; Goldberg, E. P.; Reich, S.; Dan, N. *Macromolecules* **2005**, *38*, 4254.
(6) Tadd, E. H.; Zeno, A.; Zubris, M.; Dan, N.; Tannenbaum, R. *Macromolecules* **2003**, *36*, 6497.
(7) Heck, R. F.; Breslow, D. S. *J. Am. Chem. Soc.* **1961**, *83*, 4023.
(8) Ungváry, F.; Markó, L. *J. Organomet. Chem.* **1969**, *20*, 205.
(9) Werner, P.; Ault, B. S.; Orchin, M. *J. Organomet. Chem.* **1978**, *162*, 189.
(10) Klaubunde, K. J.; Tanaka, Y. *J. Mol. Catal.* **1983**, *21*, 57.
(11) Kanai, H.; Tan, B. J.; Klaubunde, K. J. *Langmuir* **1986**, *2*, 760.
(12) Sauer, B. B.; Dee, G. T. *Macromolecules* **1994**, *27*, 6112.
(13) Dee, G. T.; Sauer, B. B. *Adv. Phys.* **1998**, *47*, 161.
(14) Van Der Voort, P.; van Welzenis, R.; de Ridder, M.; Brongersma, H. H.; Baltes, M.; Mathieu, M.; van de Ven, P. C.; Vansant, E. F. *Langmuir* **2002**, *18*, 4420.
(15) Nehring, J. L.; Heinekey, D. M. *Inorg. Chem.* **2003**, *42*, 4288.
(16) Chertihin, G. V.; Saffel, W.; Yustein, J. T.; Andrews, L.; Neurock, M.; Ricca, A.; Bauschlicher Jr., C. W. *J. Phys. Chem.* **1996**, *100*, 5261.
(17) Widegren, J. A.; Aiken, J. D. III; Özkar, S.; Finke, R. G. *Chem. Mater.* **2001**, *13*, 312.
(18) Griffith, P. R.; de Haseth, J. A. *Fourier Transform Infrared Spectroscopy*; John Wiley & Sons: New York, 1986.
(19) LaMer, V. K.; Dinegar, R. H. *J. Am. Chem. Soc.* **1950**, *72*, 4847.
(20) LaMer, V. K. *Ind. Eng. Chem.* **1952**, *44*, 1270.
(21) Smoluchowsky, M. V. *Z. Phys. Chem. (Munich)* **1917**, *92*, 129.
(22) McLeod, J. B. Q. *J. Math. Oxford (2)* **1962**, *13*, 119.
(23) Ziff, R. M. *J. Stat. Phys.* **1980**, *23*, 241.

MA050564T